PERGAMON

International Journal of Multiphase Flow 27 (2001) 61–87

International Journal of Multiphase Flow

www.elsevier.com/locate/ijmulflow

The calculation of inertial particle transport in dilute gas-particle flows

Shane A. Slater, John B. Young*

Whittle Laboratory, Cambridge University, Madingley Road Cambridge, CB3 0DY, UK

Received 25 June 1999; received in revised form 7 December 1999

Abstract

The paper describes a new time-marching method for calculating two-dimensional, dilute, non-turbulent, gas-particle flows using an Eulerian formulation. The method is accurate and robust, and overcomes many of the deficiencies of other schemes reported in the literature. A particular feature is the ability to calculate the particle density field accurately even in the vicinity of discontinuities, particle-free 'shadow' zones and particle separations from solid surfaces. The paper discusses the ill-posedness of the Eulerian equations and describes the numerical scheme, focusing on (i) the particle boundary condition at solid surfaces, (ii) the capture of discontinuities in the particle density field, (iii) special techniques to handle shadow zones, (iv) convergence acceleration for particle flows with very small Stokes numbers and, (v) the possibility of crossing particle trajectories. Applications of the method are illustrated by calculations of particle flow over a circular cylinder and through a turbine cascade. The results agree well with the predictions of a computationally more expensive Lagrangian tracking code and the method offers the possibility of extension to include turbulent particle transport.

Keywords: Particle transport; Deposition; Multiphase flow; Eulerian; Lagrangian tracking; Discontinuity; Shadow zone

1. Introduction

Dilute gas-particle flows are common both in natural and industrial processes. One

* Corresponding author.
E-mail address: jby@eng.cam.ac.uk (J.B. Young).

0301-9322/01/$ - see front matter
PII: S0301-9322(99)00122-6

important engineering application is in clean-coal gas turbine systems for electrical power generation where micrometre sized fly-ash particles generated by a coal gasifier or fluidised bed combustor may deposit on the turbine blade surfaces, reducing output power, efficiency and structural integrity (Wenglarz, 1981). In such cases, both inertial and diffusional mechanisms operate in concert to transport particles to the blade surfaces. Particle inertia is responsible for the deviation of the particle trajectories from the curved gas streamlines in the central passage region and also for the inability of the particles to replicate the motion of the gas eddies in the turbulent boundary layers adjacent to the blades. Within these boundary layers, particle transport by turbulent diffusion is important and, in the presence of strong temperature gradients, thermophoresis may be significant.

As a prelude to a computation involving all transport mechanisms, it is prudent to examine each phenomenon in isolation as far as this is possible. Turbulent deposition, for example, can be studied in turbulent pipe-flow, as this eliminates the complication of inertia effects due to curved streamlines. Many experimental and theoretical studies of this configuration have been made (Papervergos and Hedley, 1984) and a theory is now available (Young and Leeming, 1997) which is believed to model the physics of pipe-flow deposition in a reasonably satisfactory manner and which offers the possibility of extension to more complex situations.

The present paper concentrates on the calculation of particle transport in non-turbulent, dilute particle flows where deposition is caused entirely by particle slip generated by the streamline curvature of the carrier gas flow. (The adjective dilute implies that the gas flow is not influenced by the presence of the particles). There are two fundamentally different approaches for calculating flows of this type, referred to as the Lagrangian and Eulerian (or two-fluid) methods. In fact, both methods use standard Eulerian CFD solvers to obtain the gas flowfield but then use different techniques for calculating the particle motion.

In the Lagrangian method, the particle momentum equation is integrated numerically along particle pathlines to give the particle velocity field. This is a standard technique (e.g., Valentine and Decker, 1994) but the solution of the particle continuity equation to give the particle density field is much more difficult. The usual approach is to compute a large number of particle paths and estimate the number instantaneously resident within each computational cell of an Eulerian grid (Crowe et al., 1977). Unfortunately, however, a large computational effort is required to track the various particles needed to reduce the statistical noise in the results. The problem is compounded when a stochastic or 'random walk' element is introduced to model the effects of particle turbulence. Even with dramatic improvements in computer speed it is doubtful whether this method will ever be able to resolve the details of complex 3D particle flowfields with turbulent boundary layers. Indeed, it is conceptually unclear how the Lagrangian approach can handle diffusive fluxes resulting from turbulent fluctuations of particle density.

In the Eulerian method, the particle equations are solved in Eulerian form (e.g., Ohkawa and Tomiyama, 1994). This approach is attractive as similar techniques may be used for both phases, allowing relatively easy inclusion of two-way coupling effects. Turbulence closure models can be incorporated without the computational penalty of the Lagrangian approach and, indeed, the method has been used to predict turbulent particle transport while neglecting inertia effects due to streamline curvature (Menguturk and Sverdrup, 1981; Parker and Lee, 1972). Particle bouncing and crossing trajectories present serious difficulties but, nonetheless,

the approach provides the best vehicle for calculating particle transport when inertial and turbulent mechanisms are both important and was therefore chosen for the present study.

Eulerian schemes are not as common as their Lagrangian counterparts because they are intrinsically more difficult to develop and code. There are also a number of computational problems which have never been satisfactorily addressed in the literature. These include, (i) the implementation of surface boundary conditions, (ii) the accurate capture of density discontinuities, (iii) techniques for handling the equations in particle-free 'shadow' zones, (iv) convergence acceleration for flows at very low Stokes numbers and, (v) the thorny problem of 'crossing trajectories'. The new method cannot deal with particle reflections at solid surfaces or crossing trajectories, but otherwise provides a robust solution to all of these difficulties.

2. Basic equations

In dilute gas-particle flows, the gas-phase equations are uncoupled from the particle equations and may be solved in isolation. The problem of establishing the gas flowfield is therefore separate from the current investigation and is not discussed here.

The conservation equations of mass and momentum for the unsteady flow of mono-dispersed spherical particles may be written (using cartesian tensor notation with the repeated suffix summation convention) as,

$$\frac{\partial \rho_{\mathrm{p}}}{\partial t} + \frac{\partial \left(\rho_{\mathrm{p}} V_j\right)}{\partial x_j} = 0 \tag{1}$$

$$\frac{\partial \left(\rho_{\mathrm{p}} V_i\right)}{\partial t} + \frac{\partial \left(\rho_{\mathrm{p}} V_i V_j\right)}{\partial x_j} = \frac{\rho_{\mathrm{p}}(U_i - V_i)}{\tau_{\mathrm{p}}} \quad \text{Conservative form} \tag{2a}$$

$$\frac{\partial V_i}{\partial t} + V_j \frac{\partial V_i}{\partial x_j} = \frac{(U_i - V_i)}{\tau_{\mathrm{p}}} \quad \text{Non-conservative form} \tag{2b}$$

where ρ_{p} is the particle density (mass of particles per unit volume), V_i is the i-component of particle velocity and U_i is the i-component of gas velocity. The particle dynamic relaxation time τ_{p} is given by,

$$\tau_{\mathrm{p}} = \tau_{\mathrm{p,\ Stokes}} \left(\frac{1 + \psi\left(Kn_{\mathrm{p}}\right)}{1 + \phi\left(Re_{\mathrm{p}}\right)} \right) \tag{3}$$

where $\tau_{\mathrm{p,\ Stokes}}$ is the value for a spherical particle in Stokes flow,

$$\tau_{\mathrm{p,\ Stokes}} = \frac{d_{\mathrm{p}}^2 \rho_{\mathrm{mat}}}{18 \mu_{\mathrm{G}}} \tag{4}$$

d_{p} being the particle diameter, ρ_{mat} the particle material density and μ_{G} the gas dynamic viscosity. $1 + \phi(Re_{\mathrm{p}})$ represents a correction for finite particle slip velocities based on the local

value of the particle slip Reynolds number Re_p, and $1 + \psi(Kn_p)$ is a correction for rarefied gas effects based on the local value of the particle Knudsen number Kn_p. For the present work, the functions ϕ and ψ are specified by the empirical expressions of Morsi and Alexander (1972) and Cunningham (see Crowe et al., 1998, p. 75), respectively.

In writing the momentum equation, it has been assumed that $\rho_{mat} \gg \rho_g$ (where ρ_g is the gas density), so that the virtual mass, pressure gradient and Basset history terms can be neglected. The gravity and lift force terms have also been omitted, together with any contributions from turbulent transport mechanisms. Eqs. (1) and (2) therefore provide a simple framework suited to the investigation of inertial phenomena.

3. Ill-posedness of the particle equations

Superficially, Eqs. (1) and (2) resemble the Euler equations of gas dynamics but their behaviour is actually quite different because of the lack of a pressure gradient term in the momentum equation. The particle equations are hyperbolic and, as discussed by Fernandez de la Mora and Rosner (1981), information can only travel through the computational domain in the direction of the particle pathlines (which are the characteristics of the equations). This behaviour has important consequences because the equation set may become ill-posed. With the exception of a small body of Russian literature (e.g., Osiptsov, 1984, 1985, 1997) and sporadic Western research, such considerations have been almost completely ignored. The manifestations of ill-posedness are evident in various published studies, although often the behaviour is falsely attributed to some kind of genuine physical phenomenon.

The most obvious example of ill-posedness is when individual particle pathlines cross. This is possible because the particles do not form their own pressure field and do not respond directly to the fluid pressure. Lagrangian modelling methods can readily deal with this behaviour since each particle carries with it sufficient information to define its own velocity at the crossing point. Eulerian methods, however, work with a single 'field' value for the velocity which, in regions of crossing trajectories, represents an average value. When particle trajectories cross, Eulerian methods can sometimes generate solutions which are not only inaccurate but also physically incorrect.

Such a situation is shown in Fig. 1, which illustrates the intersection in a uniform gas flowfield of two oblique particle 'jets'. Because the particle field is assumed to be dilute, there is no interaction of the jets in the crossing region. The Lagrangian calculation can handle this situation and provides a physically correct solution with the jets emerging from the crossing region intact and the particle density in the crossing region exactly double that for a single jet. The Eulerian calculation, on the other hand, averages the two velocities in the crossing region, thus losing information about the cross-stream components. Downstream, the solution bears no resemblance to physical reality.

Fig. 2 shows a similar situation with particles rebounding from a solid surface. The flowfield is that of an inviscid gas approaching a stagnation point and the particle trajectories have been calculated from the well-known analytical solution assuming perfectly elastic collisions at the wall. In the crossing trajectory region, information is convected towards the wall by the incident flow and away from the wall by the reflected flow. A Lagrangian approach can model

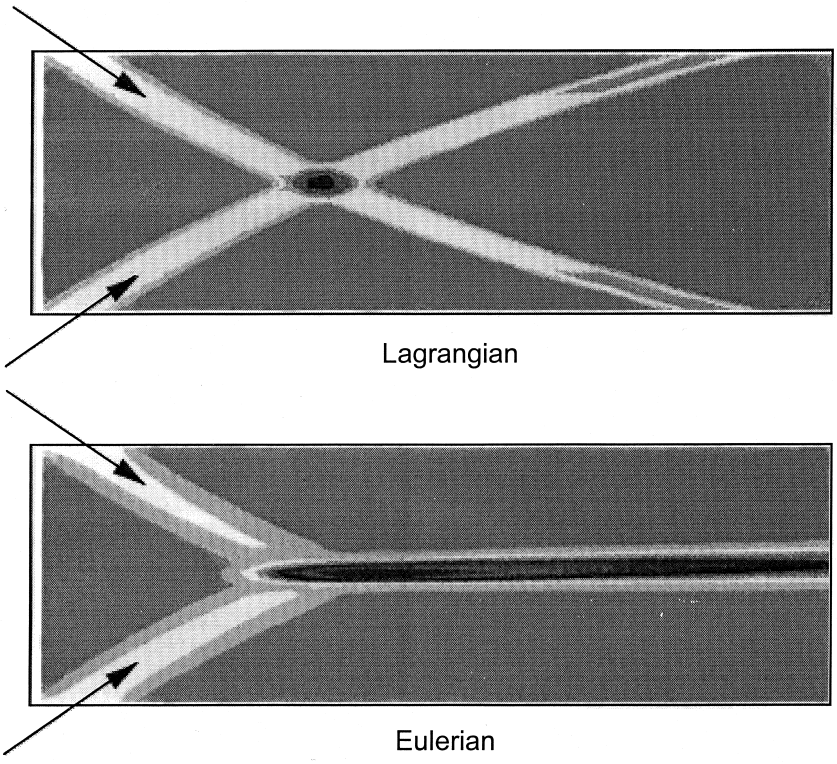

Fig. 1. Intersecting particle 'jets' in a uniform gas flow. Contours of particle density calculated by (a) Lagrangian method, (b) Eulerian method.

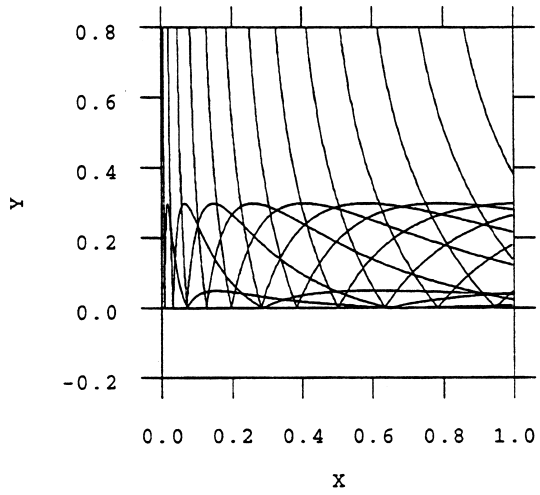

Fig. 2. Lagrangian solution of plane 2D stagnation point flow with particle rebound.

this situation correctly but the Eulerian equations cannot convect information in two or more directions simultaneously. This implies that Eulerian methods couched in terms of a *single-valued* velocity vector cannot represent *any* degree of particle reflection. The only acceptable boundary condition corresponds to a perfectly absorbing wall and (given the direction of information flow) this must be implemented in such a way that incident particles are unaware of the presence of the wall until the moment of impact.

This basic requirement is often ignored. Indeed, the most common boundary condition reported in the literature is that of a zero wall-normal particle flux (Hoffmann and Galea, 1993; Yang et al., 1993; Thai-Van et al., 1994). Sometimes this is applied in the hope of modelling perfect reflection (incident and reflected streams cancel each other out) and sometimes perfect absorption (deposited particles have zero wall-normal velocity). In practice, the zero flux condition has the undesirable effect of forcing the particle flow to turn parallel to the wall and results in a spurious increase in particle density close to the surface. Often, this is believed to represent a deposited film of particles, but actually a physically meaningless steady-state has been achieved whereby stabilising diffusive terms (modelled or artificial) drive a diffusive particle flux back into the flow, just balancing the incoming convective flux.

The only known method for modelling particle reflection correctly with a single-velocity Eulerian approach is to use the superposition technique whereby the impaction velocities from the first calculation are used to generate the initial conditions for a second, independent, calculation, and so on. The particle density fields from each calculation are then summed to give the total density (Saurel et al., 1995). This technique is not as straightforward as it sounds, however, and has only been demonstrated with comparatively simple flowfields.

It is not always appreciated that trajectory crossing can also occur in the main flowfield even when particles and carrier gas both enter the domain as uniform parallel flows. This type of situation has been analysed very instructively by Osiptsov (1984) who describes a number of cases when the particle density actually becomes infinite at singular points, lines or surfaces within the flow. Generally speaking, crossing trajectories become more likely as particle inertia increases and hence it follows that Eulerian methods may become less accurate with increasing Stokes number. In most cases, there is no way of anticipating this difficulty a priori and rudimentary Lagrangian calculations should always be performed to check for crossing trajectories if there is any doubt about the validity of the Eulerian assumptions.

Crossing trajectories represent a situation where the flow is 'over-prescribed'. Another example of ill-posedness occurs in particle-free 'shadow zones' but here the flow is 'under-prescribed'. A simple example is given in Fig. 3 which shows the variation with (non-dimensional) distance of the particle velocity and density when a uniform flow of particles are injected with a finite velocity into a stationary gas. Solving the particle mass and momentum equations analytically shows that the particle velocity decreases linearly to zero at $x = 1$ as the particle density increases without bound. The region $x > 1$ is a particle-free shadow zone. The particle flow is well-posed up to $x = 1$ but the shadow zone receives no information from the particles in the region $0 \leq x \leq 1$. In multi-dimensional flows much more complex shadow zones can form.

Lagrangian methods can deal with shadow zones easily because particles never enter the regions in question and the boundaries are defined by the limiting trajectories. Eulerian methods, on the other hand, must solve the equations over the whole domain, including

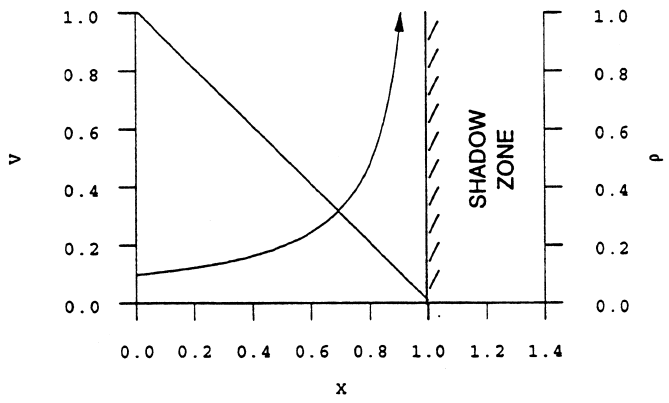

Fig. 3. 1D particle flow in a stationary gas showing the particle density discontinuity and shadow zone.

the shadow zones, as the boundaries are not known at the start of the calculation. Because shadow zones are outside the domain of dependence of the main particle flow, the Eulerian equations are under-prescribed in these regions. The mathematical implications of this fact have not been addressed in the literature to date. The solution proposed in the present work is to postulate the existence in shadow zones of a 'virtual' particle flow with density effectively zero but with a finite valued and smoothly varying velocity field. The origin of this virtual particle flow can always be traced back to solid boundaries within the shadow zone itself. It is, therefore, essential to prescribe solid surface boundary conditions for this region which will produce a virtual particle flow which will not destabilise the calculations and will also blend smoothly with the real particle flow at the shadow zone edge. It is not simple, however, to devise a boundary condition that will accurately model particle deposition in impaction regions and also generate stable virtual flows in shadow zones which are initially undefined.

Frequently, all these manifestations of ill-posedness can be found within a single flowfield.

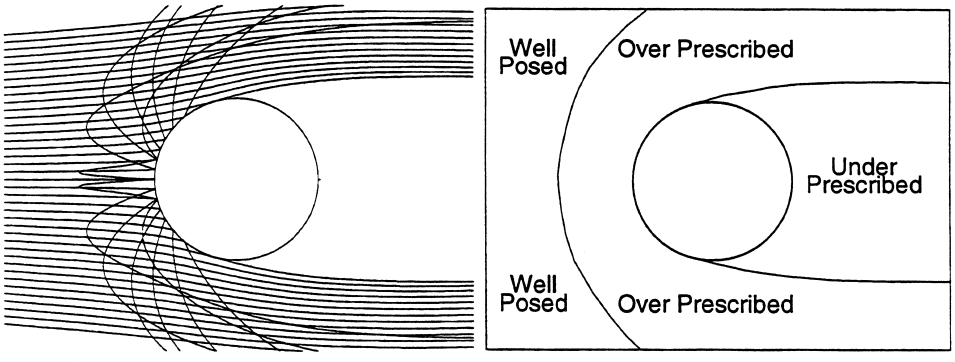

Fig. 4. Flow regimes for particle transport over a circular cylinder in an inviscid gas flow with rebound.

Fig. 4, for example, shows the over-prescribed and under-prescribed regions for particle flow (with bouncing) over a circular cylinder in a potential gas flow. This is a comparatively simple two-dimensional flowfield and bodies with more complex geometries (such as the turbine cascade analysed later in the paper) may well generate more than one shadow zone. Clearly, the requirements on an Eulerian method to produce an accurate solution of the particle equations and be robustly stable are not easy to maintain.

4. Numerical discretisation

In non-conservative form, the momentum equation (2b) does not involve the particle density ρ_p and may be solved independently of the mass equation (1) using a finite difference technique. This is the basis of the Lagrangian trajectory approach but is not to be recommended for an Eulerian method. In order to guarantee flux conservation, a finite volume rather than finite difference scheme is preferable and this necessitates writing the momentum equation in conservative form. Hence, at the expense of weakly recoupling the momentum equation, Eqs. (1) and (2a) are taken as the working forms.

The finite volume equations are generated by integrating over a computational cell of volume $\delta\Omega$ and applying Gauss's theorem. The result is,

$$\frac{\Delta\rho_p}{\Delta t}\delta\Omega = \sum_{\text{Faces}} \rho_p V_j \delta A_j \tag{5}$$

$$\frac{\Delta(\rho_p V_i)}{\Delta t}\delta\Omega = -\sum_{\text{Faces}} \rho_p V_i V_j \delta A_j + \frac{\rho_p (U_i - V_i)}{\tau_p}\delta\Omega \tag{6}$$

where δA_j is the projection in the j-direction of the vectorial area of a cell face and the summation is over all the faces enclosing the volume $\delta\Omega$. A forward-difference time-derivative is implied by the notation $\Delta p_\rho/\Delta t$ and $\Delta(p_\rho V_i)/\Delta t$.

Eqs. (5) and (6) are applied to every cell of a two-dimensional structured grid, an example of which is shown in Fig. 5. The equations are then marched forward in time, updating the values of ρ_p and $\rho_p V_i$ at every step, until a steady-state is achieved. Cell centred storage is used and, for internal cells, the fluxes of mass and momentum crossing the faces are calculated from the linear average of the variables stored at adjacent cell centres. On a cartesian mesh with uniform grid spacing, this is equivalent to second-order accurate central differencing. It would be a straightforward task to improve accuracy on a non-uniform mesh by using weighting functions based on grid geometry (Hirsch, 1990) but this is hardly necessary if the grid spacing changes slowly.

The choice for flux evaluation may be seen as somewhat contrary to the flow physics and it is necessary to restore the hyperbolicity of the governing equations through the introduction of artificial diffusion terms as described below. This approach is preferable to the fully upwinded schemes more usually employed (Ohkawa and Tomiyama, 1994; Yang et al., 1993) as the flux

evaluations are symmetrical and the order of accuracy is higher. In any case, artificial diffusion is required for the stable capture of particle density discontinuities.

5. Artificial diffusion

The form of artificial diffusion applied to the basic equations is crucial in finding a good balance between accuracy and stability. A 'tuneable' diffusivity is needed to provide a controlled amount of low-level upwinding over most of the flowfield but an increased level near particle density discontinuities so that these features are captured in a stable and accurate manner. To this end, a form of artificial diffusion is used which is similar to that developed by Jameson et al. (1981) for shock capturing in supersonic gas flows. This involves adding explicit second- and fourth-order artificial diffusion terms to the conservation equations.

With reference to Fig. 6, a term ADF representing the sum of four artificial diffusive fluxes through the cell faces is added to the right-hand sides of each of Eqs. (5) and (6):

$$\mathrm{ADF} = AF_{\mathrm{E}} - AF_{\mathrm{W}} + AF_{\mathrm{N}} - AF_{\mathrm{S}} \tag{7}$$

where,

$$AF_{\mathrm{E/W}} = \left(D_{2\xi} \frac{\partial \phi}{\partial \xi} \Delta\eta + D_{4\xi} \frac{\partial^3 \phi}{\partial \xi^3} \Delta\eta \right)_{\mathrm{E/W}}$$

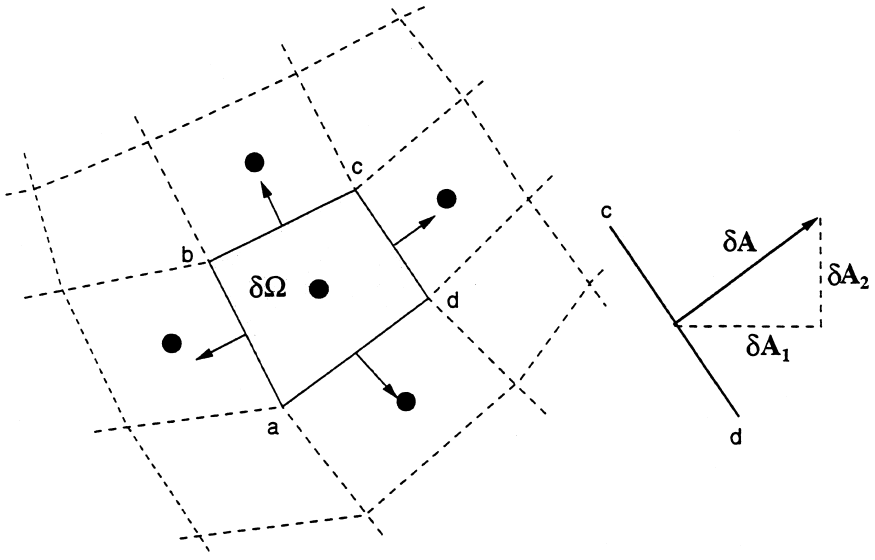

Fig. 5. Details of the 2D computational grid.

$$AF_{\mathrm{N/S}} = \left(D_{2\eta} \frac{\partial \phi}{\partial \eta} \Delta\xi + D_{4\eta} \frac{\partial^3 \phi}{\partial \eta^3} \Delta\xi \right)_{\mathrm{N/S}} \tag{8}$$

The variable ϕ represents, in turn, ρ_p and each of the components $\rho_\mathrm{p} V_i$. It should be noted that these expressions ignore the fact that the local (ξ, η) coordinate system may not be orthogonal. This is not important, however, as the artificial fluxes are small and are only included to stabilise the calculation. The artificial diffusivities are defined by,

$$D_{2\xi} = \varepsilon_{2\xi} \Delta\xi^2, \qquad D_{4\xi} = \varepsilon_{4\xi} \Delta\xi^4$$

$$D_{2\eta} = \varepsilon_{2\eta} \Delta\eta^2, \qquad D_{4\eta} = \varepsilon_{4\eta} \Delta\eta^4 \tag{9}$$

with the second- and fourth-order coefficients given by,

$$\varepsilon_{2\xi} = \frac{\beta_2}{\Delta t_\xi} \left| \frac{\partial^2 \rho_\mathrm{p}}{\partial \xi^2} \right| \frac{\Delta\xi^2}{4\rho_\mathrm{p}}, \qquad \varepsilon_{4\xi} = \max\left(0, \frac{\beta_4}{\Delta t_\xi} - \varepsilon_{2\xi}\right)$$

$$\varepsilon_{2\eta} = \frac{\beta_2}{\Delta t_\eta} \left| \frac{\partial^2 \rho_\mathrm{p}}{\partial \eta^2} \right| \frac{\Delta\eta^2}{4\rho_\mathrm{p}}, \qquad \varepsilon_{4\eta} = \max\left(0, \frac{\beta_4}{\Delta t_\eta} - \varepsilon_{2\eta}\right) \tag{10}$$

where β_2 and β_4 are user-specified coefficients (typically 0.1 and 0.01, respectively), and Δt_ξ and Δt_η are directionally dependent time scales discussed below. In Eqs. (8) and (10), all partial derivatives are represented by central differences.

From Eqs. (9) and (10), it can be seen that the second-order diffusivities $D_{2\xi}$ and $D_{2\eta}$ are proportional to the corresponding second derivatives of ρ_p. Normally, therefore, the second-

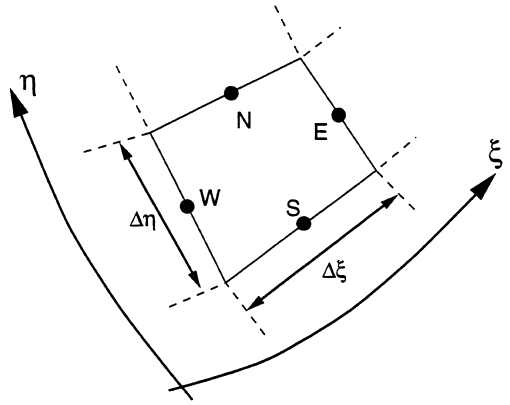

Fig. 6. Definition sketch for artificial diffusive fluxes.

order diffusive terms are only activated near shadow zone boundaries where the density curvature is high. The fourth-order fluxes are used to damp any numerical 'wiggles' in the main flowfield caused by odd–even decoupling of the numerical scheme. The form of $D_{4\xi}$ and $D_{4\eta}$ ensures that these fluxes are suppressed in regions of high density curvature where they can have a destabilising influence.

The directionally dependent time scales Δt_ξ and Δt_η are calculated from the prescription,

$$\left(\Delta\eta\frac{\Delta\xi}{\Delta t_\xi}\right)_{\mathrm{E/W}} = \left(\frac{\text{Convective mass flux}}{\rho_\mathrm{p}}\right)_{\mathrm{E/W}}$$

$$\left(\Delta\xi\frac{\Delta\eta}{\Delta t_\eta}\right)_{\mathrm{N/S}} = \left(\frac{\text{Convective mass flux}}{\rho_\mathrm{p}}\right)_{\mathrm{N/S}} \tag{11}$$

By linking the magnitude of the artificial flux to the real convective flux, the artificial diffusivities are rendered anisotropic. This is highly beneficial as it ensures that smoothing is applied only in directions where it is required and that the artificial diffusion operates correctly even on highly stretched meshes.

6. Boundary conditions

As discussed previously, the only physically meaningful solid surface boundary condition applicable when the particle equations are written in terms of a single-valued velocity vector is that corresponding to perfect absorption. This is the condition implemented here.

The physical requirement of an absorbing boundary condition must allow the wall-normal particle flux at the surface to change in response to local flow conditions. This can be formulated in a number of different ways. For example, Saurel et al. (1995) and Hussainov et al. (1996) enforced zero wall-normal gradients of particle density and velocity in order to generate the required particle fluxes at the boundary. This corresponds to a zeroth order extrapolation from the flow to the wall, but a first order scheme (where the wall-normal *gradients* are extrapolated) is more accurate and is the method adopted here. Higher order extrapolations can be devised but are more prone to instability.

Gradient extrapolation is stable when the particle velocity vector points towards the wall. If the vector points away from the wall, however, extrapolation to the boundary corresponds to a downwinded flux evaluation and is unconditionally unstable. This situation can arise, not only as an unphysical fluctuation during the transient phase of the calculation, but also as a genuine part of the steady-state solution on solid boundaries within shadow zones. In such cases, the 'virtual' particle flow in the shadow zone is not unique and depends on the boundary conditions applied at the wall. One way of fixing the solution stably is to impose a zero *wall-normal* particle flux at the boundary. The particle velocity component parallel to the wall may still be non-zero and this provides continuity of velocity, at the wall, between the real and virtual flows on either side of a particle separation line. At such points, it is found that ρ_p in

the cell adjacent to the wall decreases with time and tends to zero. This low density region then convects through the flow domain and establishes the shadow zone.

As the direction of the local particle velocity vector may change as the calculation proceeds, it is not known a priori which boundary condition to impose at any particular point along a wall. The choice must therefore be made automatically at each time-step. Referring to Fig. 7, a gradient extrapolation is first performed to all the solid walls and the resulting wall-normal particle flux is calculated. If this is directed towards the wall, gradient extrapolation is stable and the flux is unchanged. If it is directed away from the wall, a zero wall-normal flux condition is imposed. This boundary condition yields singularity-free steady-state solutions which are stable even within shadow zones.

7. Under-relaxation

Shadow zones may form, either at solid boundaries as described above, or internally within the flow (e.g., particles centrifuging out from the centre of a fluid vortex) and the numerical procedure must therefore be capable of predicting large regions where $\rho_p \to 0$. Without special treatment, however, the numerical procedure does not guarantee positivity of density and zero or negative values may appear with catastrophic results. To avoid this problem, a simple form of temporal under-relaxation is used to damp large changes in ρ_p when ρ_p is itself small. The change $\Delta\rho_p$ calculated from Eq. (5) is thus modified according to the prescription,

$$\Delta\rho_{p,\,\mathrm{mod}} = \frac{\Delta\rho_p}{1 + DF\left|\dfrac{\Delta\rho_p}{\rho_p - \rho_{p,\,\min}}\right|} \tag{12}$$

where $DF > 1$ is a user-specified damping factor (typically $DF \cong 2$). This ensures that the final updated value of ρ_p is always greater than $\rho_{p,\,\min}$ the lowest density desired in the calculation (typically set at ten orders of magnitude less than the particle density at flow inlet). Eq. (12) shows that if $\Delta\rho_p$ is negative, ρ_p approaches this minimum value asymptotically. Similar

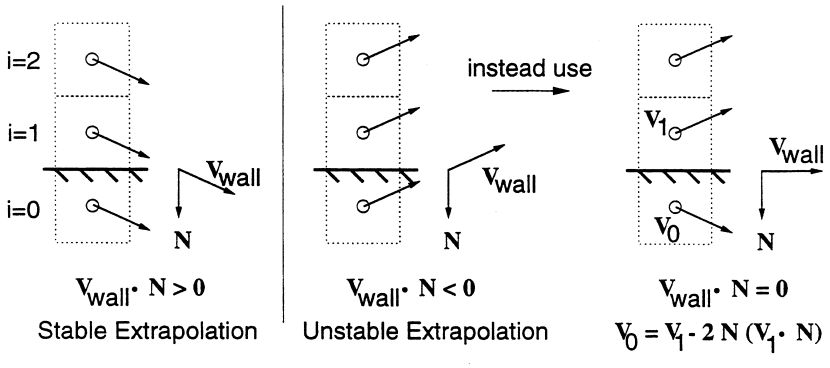

Fig. 7. Boundary conditions at a solid surface.

damping is applied to the values of $\Delta(\rho_p V_i)$ to retain stability. The increase in CPU time resulting from the application of this stabilising technique was found to be minimal.

8. Stability and convergence acceleration

A von Neumann stability analysis of the numerical scheme shows that a necessary condition for stability of the one-dimensional equations is,

$$\sigma = \frac{V\Delta t}{\Delta x} < 1 \tag{13}$$

where V is the particle velocity, Δt is the time-step and Δx is the grid spacing, all terms being evaluated locally. This is the expected CFL condition, implying that the computational velocity $\Delta x/\Delta t$ should not exceed the particle convective velocity V. Replacing the single time-stepping procedure by a four-step Runge–Kutta integration allows the use of a larger time-step ($\sigma < 2.7$) but the effective improvement is minimal because of the increased computational effort involved. The convergence rate can be improved, however, by the use of non-uniform time-steps based on the local application of Eq. (13). This is permissible if only the steady-state solution is required and time accuracy is of no importance.

The analysis also shows that, because of the drag term in the momentum equation, a further necessary condition for stability is,

$$\Delta t < \tau_p \tag{14}$$

Clearly, this requirement can seriously delay convergence for particles with small τ_p and a number of studies (Ohkawa and Tomiyama, 1994; Young and Leeming, 1997) have advocated

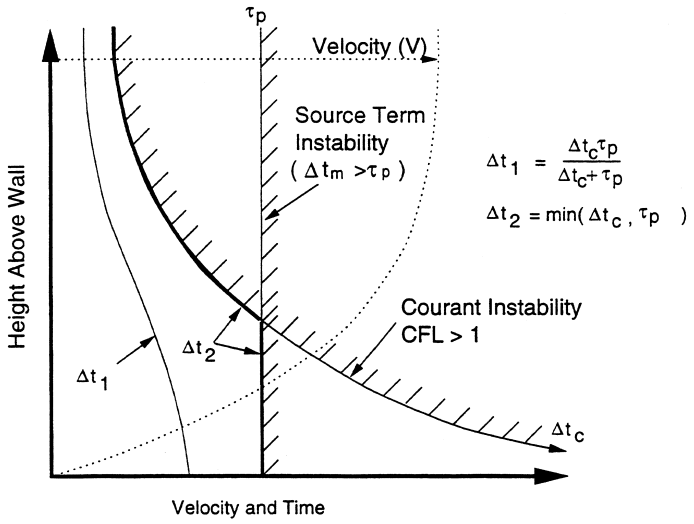

Fig. 8. Schematic diagram showing time-step limitation for flow in a boundary layer.

an implicit evaluation of the drag term in an attempt to overcome the problem. Unfortunately, the implicit procedure can be shown to be exactly equivalent to an explicit method with a modified time step given by,

$$\Delta t_{\mathrm{mod}} = \frac{\tau_{\mathrm{p}} \Delta t}{\tau_{\mathrm{p}} + \Delta t} \tag{15}$$

where Δt is calculated from Eq. (13) with $\sigma = 1$. Instead of speeding convergence, the procedure automatically limits the computational time step in such a way that $\Delta t_{\mathrm{mod}} < \tau_{\mathrm{p}}$.

In fact, the stability limit imposed by the drag term gives rise to problems which are not restricted to particle flows with small τ_{p}. Fig. 8, for example, is a schematic representation of the flow of particles in a boundary layer. As the gas (and hence particle) velocity decreases near the wall, the time step Δt (for $\sigma = 1$, say) increases at a rate inversely proportional to V (assuming constant grid spacing Δx). Irrespective of the value of τ_{p}, however, a point is eventually reached where Δt calculated from Eq. (13) exceeds τ_{p}. The maximum stable time-step is now τ_{p} and the effective value of σ drops from unity at this point to near-zero at the wall. The convergence rate in this region is therefore seriously retarded.

Problems stemming from the drag-stability requirement can be overcome by the use of different computational time-steps in the mass and momentum conservation equations. Consider the one-dimensional particle continuity equation,

$$\frac{\partial \rho_{\mathrm{p}}}{\partial t} + \frac{\partial \left(\rho_{\mathrm{p}} V\right)}{\partial x} = 0 \tag{16}$$

When V is constant, the solution is $\rho_{\mathrm{p}} = \text{constant}$ along the characteristics $\mathrm{d}x/\mathrm{d}t = V$. Assuming $|U - V| \ll |U|$, this implies that density waves propagate through the domain at approximately the local gas flow velocity. A stability analysis then shows that, for an explicit numerical method, the time-step is limited by the CFL condition, $\Delta t_{\mathrm{c}} < \Delta x/U$. If a much smaller time-step is used as a result of the drag-stability limitation of the momentum equation, the convection of density waves will be dramatically slowed. Indeed, if $\Delta t_{\mathrm{c}} \cong \tau_{\mathrm{p}}$ and $\tau_{\mathrm{p}} \rightarrow 0$, the convergence time becomes infinite. This seems unsatisfactory because the continuity equation (in isolation) is not affected by the drag-stability issue.

Consider now the one-dimensional momentum equation in non-conservative form,

$$\frac{\partial V}{\partial t} + V \frac{\partial V}{\partial x} = \frac{U - V}{\tau_{\mathrm{p}}} \tag{17}$$

For the special case where the gas velocity U is constant, the solution is,

$$U - V = (U - V)_0 \exp\left(-t/\tau_{\mathrm{p}}\right) \tag{18}$$

where t is the time measured in a Lagrangian sense along the particle pathline. The slip velocity therefore decays to its local equilibrium value with a timescale of the order τ_{p} and this is the origin of the drag-stability limitation. A stability analysis shows that explicit numerical integration of the momentum equation in Eulerian form requires $\Delta t_{\mathrm{m}} \cong \tau_{\mathrm{p}}$.

These considerations therefore suggest that Δt_{c} should be governed by the CFL condition

while Δt_m should be limited by the relaxation time τ_p in cases where $\tau_p < \Delta t_c$. This is essentially the procedure adopted but care must be taken with the numerical implementation. Thus, the continuity equation (5) is applied with a time step Δt_c to obtain a density change $\Delta\rho_{p,c}$ which is used to update ρ_p. Similarly, the i-component momentum equation (6) is applied with a time-step Δt_m to obtain the change $\Delta(\rho_p V_i)$ which is used to update $(\rho_p V_i)$. The velocity change ΔV_i is also required in order to calculate an updated value of V_i for the next momentum flux

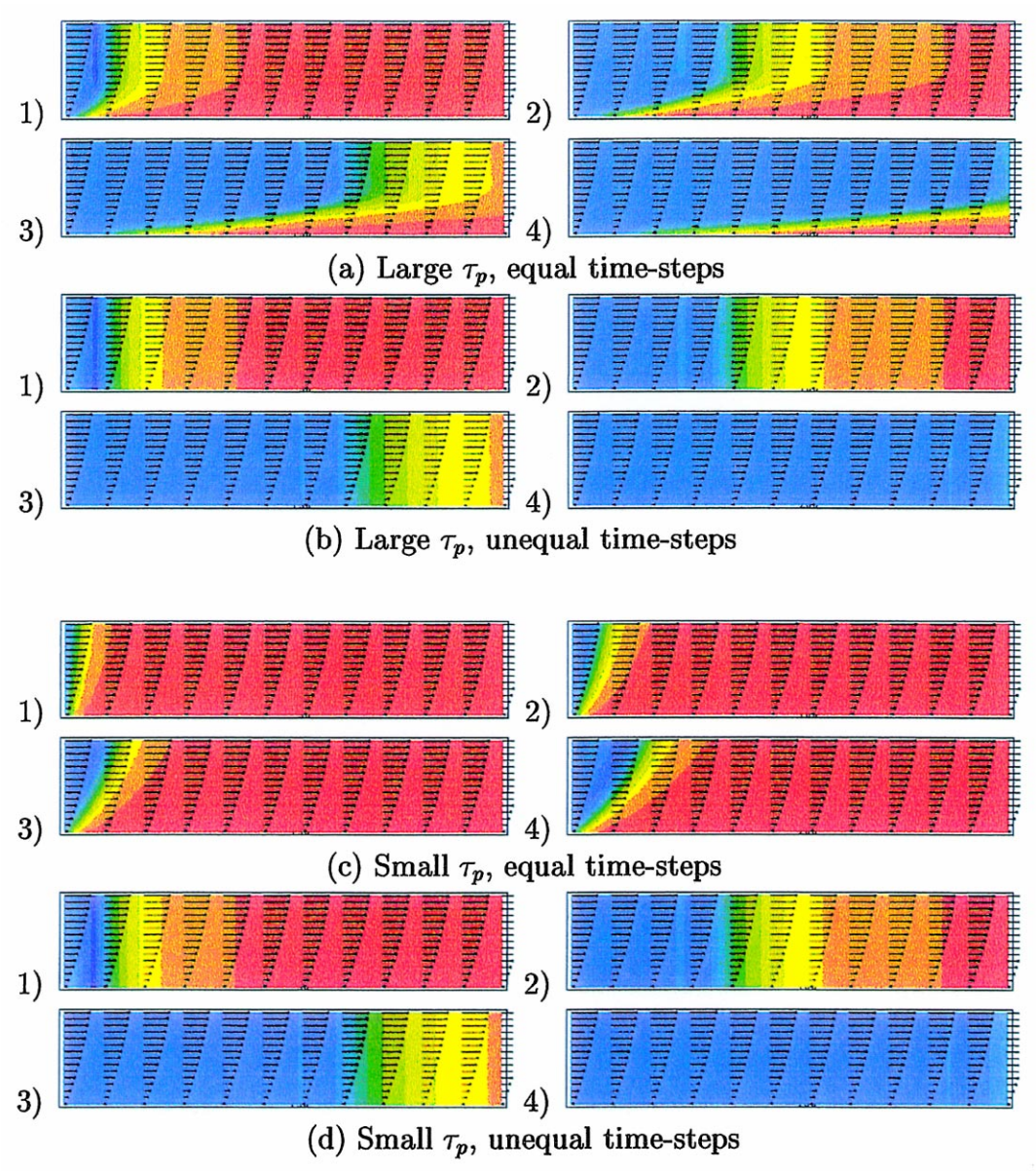

Fig. 9. Convection of density waves in a boundary layer.

evaluation and is obtained by writing,

$$\rho_p \Delta V_i = \Delta\left(\rho_p V_i\right) - V_i \Delta\rho_{p,m} \tag{19}$$

where, for consistency, $\Delta\rho_{p,m} = \Delta\rho_{p,c}(\Delta t_m/\Delta t_c)$. This procedure makes possible the calculation of particle flows with very small τ_p which otherwise would be precluded by the inordinately long CPU times required to obtain convergence.

An example is shown in Fig. 9. Particles were computationally injected into a laminar boundary layer with a slip velocity of zero and a uniform particle density of unity. The results of four separate calculations are shown and, for each calculation, four plots are presented which chart the temporal development of the density field. Fig. 9(a) and (b) refer to particles with relatively large τ_p, chosen so that the crossover point where $\Delta t_c = \tau_p$ occurred approximately half-way through the layer. Above this point, the method with equal time-steps has no trouble in propagating the flow of information. Since σ is held constant in this region, the computational wave propagation velocity is not a function of distance from the wall and the wave propagates uniformly. Below the crossover point, σ decreases as V^{-1} and the propagation of information from the inlet is delayed. The method with unequal time-steps shows no such limitation and the density wave propagates through the whole layer with the same velocity. At smaller τ_p (Fig. 9(c) and (d)), the difference is more acute. Propagation of the density wave is extremely slow using equal time-steps, while the method with unequal time-steps is unaffected by the magnitude of τ_p.

9. Lagrangian tracking

A Lagrangian particle tracking program was also written to assess the accuracy of the Eulerian method and was applied to the same test cases described in subsequent sections. The Lagrangian method is well documented (e.g., Crowe et al., 1977; Valentine and Decker, 1994) and few details are required here. The present code uses bi-linear interpolation to calculate the local gas velocity components within a cell. A simple first-order, forward-difference, time derivative is used since accuracy is maintained by integrating over the necessarily small time steps required to achieve good spatial continuity of the cell-averaged values of ρ_p and the V_i (which are calculated after all the particles have been tracked through the domain).

10. Particle flow over a circular cylinder

Particle transport in a gas flow over a circular cylinder provides a good illustration of many of the features discussed in previous sections. This test case was used solely for the purpose of developing and refining the numerical calculation procedure and no attempt was made to model the gas flowfield realistically. Accordingly, the velocity field was computed using an inviscid compressible Euler solver which, of course, could not reproduce the boundary layers on the cylinder surface nor the unsteady separated wake flow. Accepting this flowfield as a

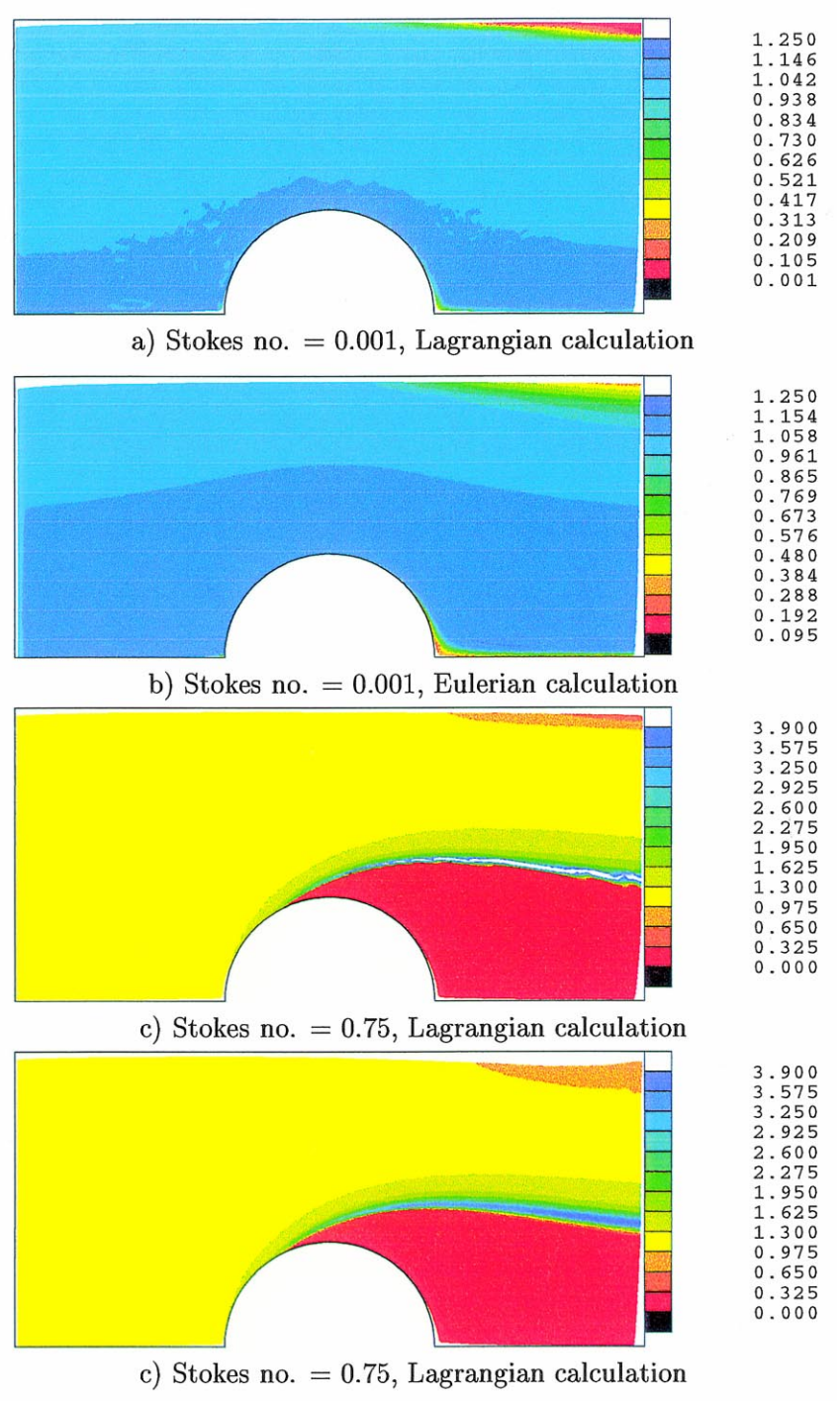

Fig. 10. Particle transport over a cylinder in an inviscid gas flow. Contours of particle density.

basis, the Eulerian and Lagrangian particle codes were then used to compute the transport of particles injected uniformly at the inlet boundary with zero slip velocity.

Fig. 10 shows a comparison between the particle density fields computed by the Eulerian and Lagrangian methods for mono-dispersed particles with diameters of 5 and 150 μm. The corresponding Stokes numbers (based on the cylinder diameter and free stream flow velocity) are 0.001 and 0.75, respectively. For the 5 μm particles (Fig. 10(a) and (b)), the velocity slip is very small and the trajectories only deviate from the (inviscid) gas flow near the rear stagnation point where a tiny shadow zone is formed. Despite the fact that 10,000 particle trajectories were used for the Lagrangian calculation, some statistical scatter is still plainly visible in Fig. 10(a). Clearly, extending the technique for use in three-dimensional geometries is likely to incur prohibitive computational penalties if accurate predictions of density fields are required. The Eulerian calculation, on the other hand, generates a smooth density field with only moderate computational effort (Fig. 10(b)). This was achieved using unequal time-steps in the mass and momentum equations as described previously. A calculation using equal time-steps is not a practical option at such small Stokes numbers because of the enormous CPU time required to obtain convergence.

The calculation for the 150 μm particles is not affected by convergence issues but has its own special problems because the particles separate from the cylinder much earlier and the shadow zone covers a very large portion of the computational domain. Fig. 10(c) and (d) show that both methods generate similar density fields. In the shadow zone, the Lagrangian calculation predicts a particle density of exactly zero simply because no trajectories enter the region. The Eulerian calculation converges to a value which is ten orders of magnitude less than that in the free-stream (but is still, nevertheless, finite and positive). This near-zero, but finite, density is established stably throughout the 'virtual' particle flow in the shadow zone and demonstrates the effectiveness of the under-relaxation technique described previously. The particle velocity vectors from the Eulerian calculation are shown in Fig. 11(a). On the upstream side of the cylinder, the particles reach the surface with a finite wall-normal component of velocity and inertially deposit. Moving along the cylinder surface in the downstream direction, the wall-normal component of velocity decreases until the particle flow is tangential to the surface. This defines the start of the shadow zone. Downstream of this point, the velocity near the wall points away from the surface and the zero wall-normal mass-flux boundary condition is activated automatically, avoiding any spurious entrainment of particles from the flow boundary. The particle velocity throughout the shadow zone is well-behaved, even as $\rho_p \rightarrow 0$. Fig. 11(b) shows the percentage difference in particle velocity between the Lagrangian and Eulerian calculations. Clearly the agreement is excellent, the differences rarely exceeding 0.25%. Indeed, it is generally found that agreement between the velocity fields is, if anything, slightly better than between the density fields.

One of the most challenging tasks for an Eulerian solver is the accurate prediction of the density profile across the discontinuous transition at the edge of a shadow zone. Characteristically, trajectories tend to 'bunch up' in these regions resulting in values of ρ_p which may be many times higher than those in the free-stream. This behaviour is shown graphically in Fig. 12(a) for the 150 μm particles. The Lagrangian calculation predicts a peak particle density, some four times the free-stream value, followed by a genuinely discontinuous transition to a density of precisely zero in the shadow zone. The Eulerian calculation, on the

other hand, shows significant smoothing, an effect which is due almost entirely to the coarseness of the grid rather than the artificial diffusion. (In fact, the anisotropy of the artificial diffusion ensures that its magnitude normal to the convective particle flow direction is near-zero.) In order to improve the resolution near the edge of the shadow zone a simple technique was used whereby each gridline connecting two mesh points was notionally replaced by a spring with a spring constant related to the local magnitude of $\nabla\rho_p$. In regions of high $|\nabla\rho_p|$, the springs contracted the grid thus increasing the density of points where required while retaining a structured mesh with the same number of cells overall. Fig. 13 shows the original and modified grids, and Fig. 12(b) shows the very significant improvement in the Eulerian prediction of the particle density profile near the edge of the shadow zone. The average change in density across the discontinuity is almost an order of magnitude per computational cell. It is

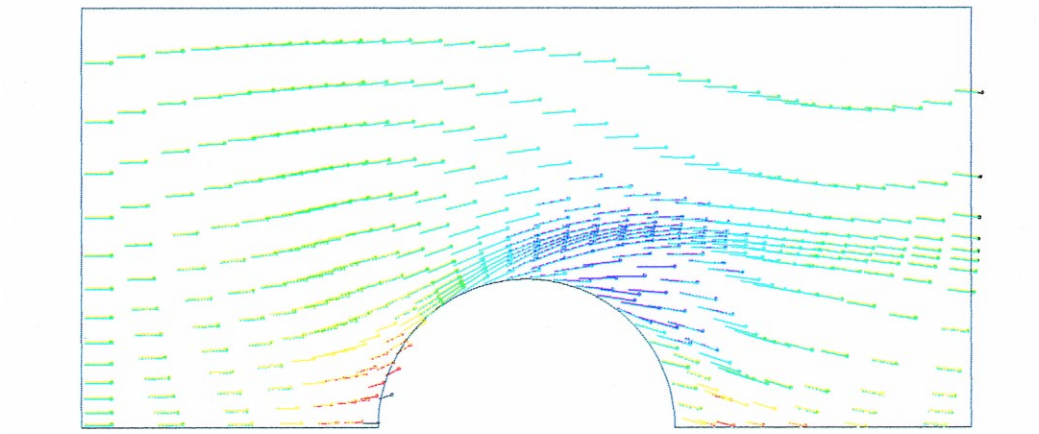

(a) Particle velocity vectors; Eulerian predictions.

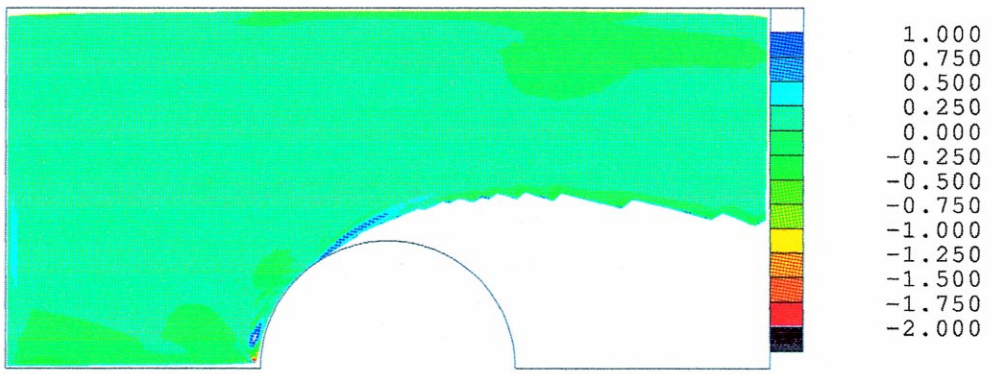

(b) Percentage error between Eulerian and Lagrangian predictions of velocity; (the shadow region is not contoured as it contains no Lagrangian velocity data).

Fig. 11. Eulerian and Lagrangian particle velocities, Stokes no. = 0.75.

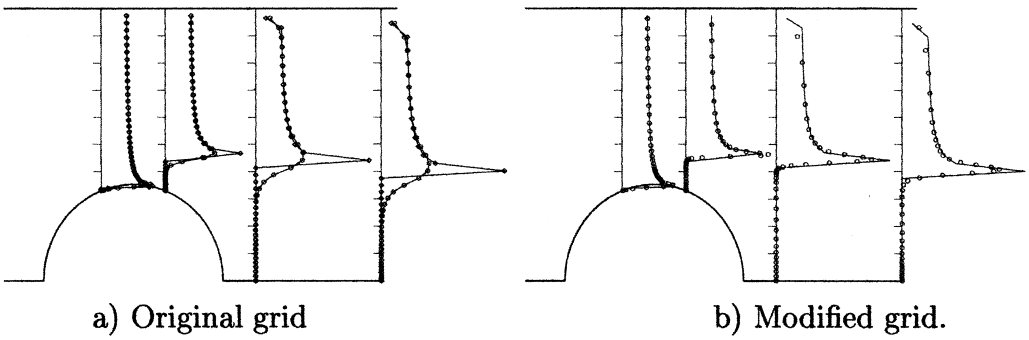

Fig. 12. Particle density profiles at the shadow zone boundary (Stokes no. = 0.75) (———) Lagrangian, (•) Eulerian.

also worth noting that the use of 'flux-limiting' schemes which try to remove false Gibbs-phenomenon-like overshoots at discontinuities would find it difficult to avoid smoothing the sharp density peak associated with trajectory bunching which is such a characteristic of these regions.

A comparison of the Eulerian and Lagrangian predictions of particle density and deposition rate on the cylinder surface are shown in Fig. 14, plotted as functions of angle from the forward stagnation point. Fig. 14(a) shows results for the 5 μm particles. Both methods predict

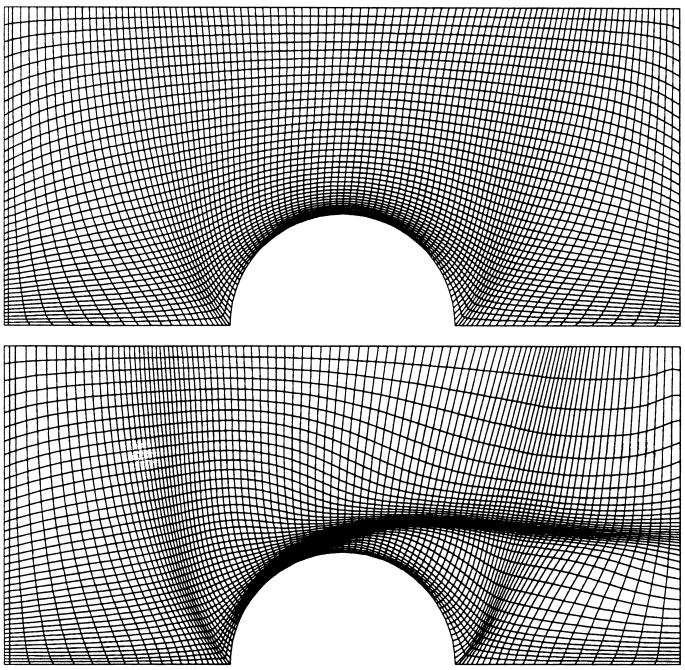

Fig. 13. Original and modified computational grids.

a reduction in ρ_p at the stagnation point which is incorrect as ρ_p should become infinite for subcritical Stokes numbers (Taylor, 1940). However, the particle pathlines near the stagnation point have very high curvature and this effect can only be captured by employing an inordinately fine computational mesh. Away from the stagnation point, the flow recovers quickly and the Eulerian method predicts a smoothly decreasing particle density around the cylinder. This is in keeping with the very slight centrifuging effect which establishes the thinnest of shadow zones adjacent to the cylinder surface. The Eulerian method is able to recognise this and activates the zero wall-normal particle flux boundary condition which, in turn, results in the (correct) prediction of a zero deposition rate over the whole cylinder surface. In contrast, the Lagrangian method has great difficulty in handling such small slip velocities and accumulates numerical errors which are responsible for the unphysical behaviour of the particle density from about 60° and the four 'rogue' deposition points. Fig. 14(b) shows the results for the 150 μm particles. Both methods give virtually identical results for particle density and deposition rate, except near the particle separation point where the Eulerian method displays a slight smoothing as the density approaches zero.

The prediction of shadow zones is such a vital and challenging aspect of Eulerian particle calculations that it is instructive to examine their temporal evolution. Fig. 15 shows contour plots of ρ_p and particle velocity vectors at a series of time-steps from the initial guess for the 150 μm particle flow over the cylinder. The transient solution is not, of course, time-accurate. From an initial guess of $\rho_p = 0.5$ throughout the field, the wave of particles with $\rho_p \cong 1$ convecting from the inlet is apparent. In the early stages, as a result of centrifuging, many velocity vectors adjacent to the cylinder point from the wall back into the flow. This automatically activates the zero wall-normal mass flux boundary condition and, after 60 time-steps, these vectors cover approximately two-thirds of the cylinder surface. As a result, particles leave wall adjacent cells but cannot enter, and ρ_p drops. Regions of low density quickly form, are convected in the downstream direction to form the shadow zone and, after about 300 time-steps, the flow is fully developed. Clearly, the success of such a calculation is

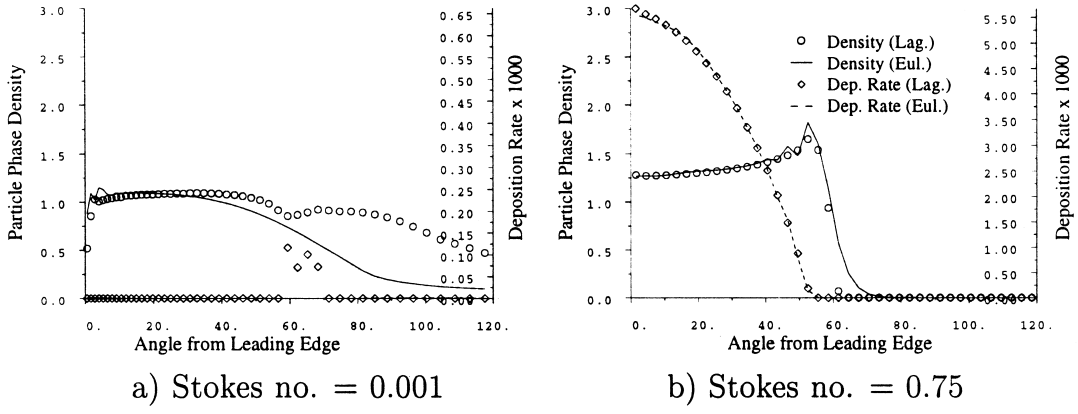

Fig. 14. Variation of particle density and deposition rate on the cylinder surface.

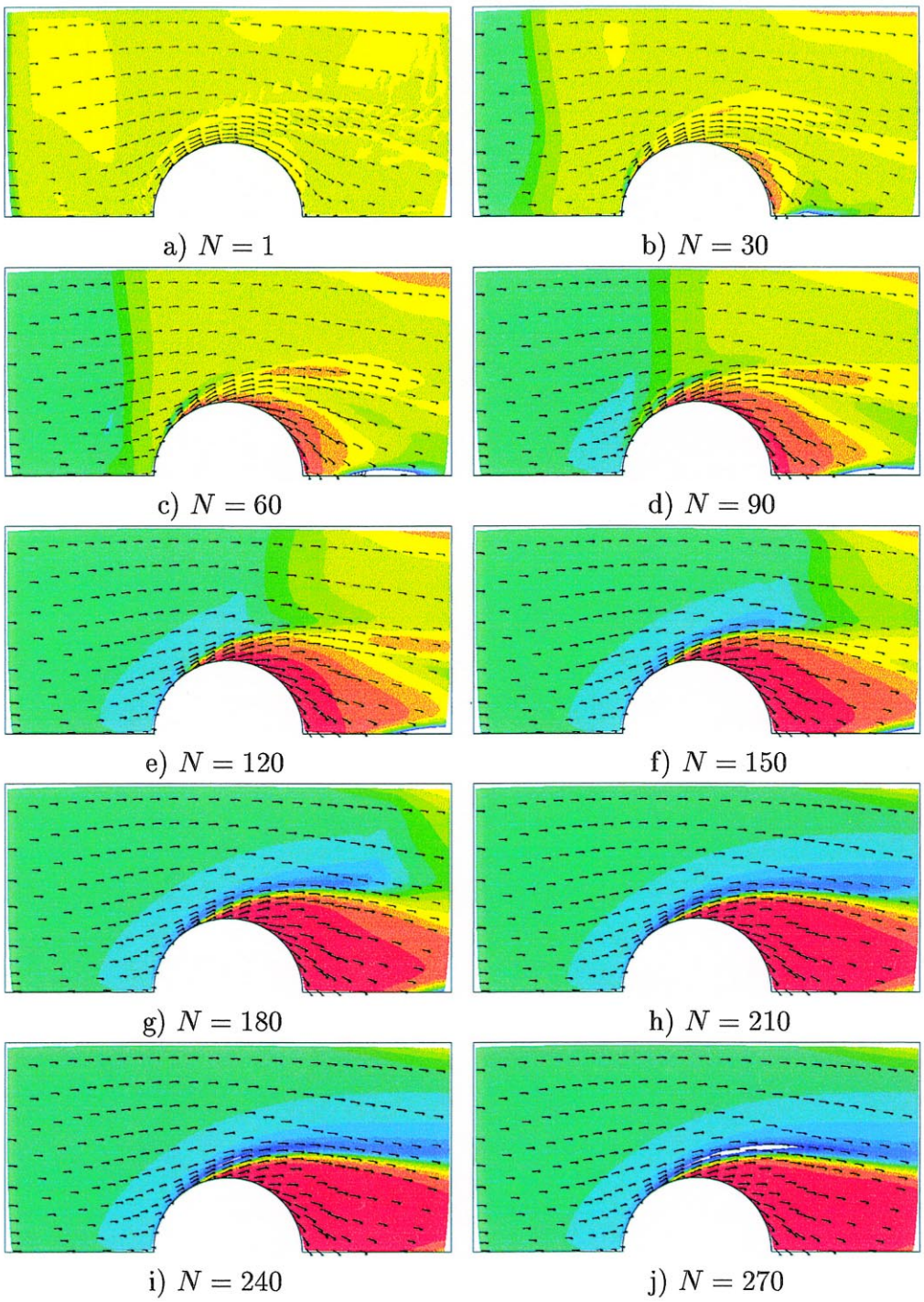

Fig. 15. Temporal evolution of the shadow zone (Stokes no. = 0.75, Eulerian calculation).

very dependent on the ability of the wall boundary extrapolation to respond to local flow conditions in the correct manner.

11. Particle transport in a turbine cascade

Predicting the transport of particulates through a turbine cascade is an engineering problem of interest to both the steam and gas turbine industries (i.e., the deposition of water droplets on wet steam turbine blades and the deposition of ash particles in coal-fired gas turbines). Because of the practical importance and also as an example of a more complex flowfield, results are now presented for particle flow through a turbine blade passage.

The chosen blade was a NASA TN D-3751 profile which was used in a Von Karman Institute workshop on multi-dimensional flow calculations. The gas flowfield at the design condition was calculated using an inviscid Euler solver so that the effects of streamline curvature could be assessed without the presence of the boundary layers. The Eulerian and Lagrangian methods were then used to calculate the transport of 6 μm particles through the cascade, corresponding to a Stokes number of 12 (based on the blade chord length and exit flow velocity). Particles were assumed to enter the cascade with $\rho_p = 1$ and zero slip velocity.

Initial tests with the Lagrangian tracking code indicated that the statistical convergence of the particle density field to an accuracy of $\pm 1\%$ required a prohibitively large number of particle trajectories. This was mainly due to the very fine mesh spacing near the blade surface used to capture the high velocity gradients at the leading and trailing edges. Relaxing the criterion to $\pm 10\%$ resulted in a requirement of 50,000 trajectories which was deemed acceptable. (Once again, this highlights the computational penalties associated with extending Lagrangian methods to three-dimensional geometries.)

Fig. 16 shows the Eulerian and Lagrangian calculations of the particle density field. The spatial extents of the shadow zones are almost indistinguishable and the only substantial difference between the two calculations is the smearing of the high density gradients in the Eulerian simulation. As with the particle flow over the cylinder, there is considerable 'trajectory bunching' resulting in high values of ρ_p near the shadow zone boundary. Fig. 17 shows magnified views of the Eulerian and Lagrangian particle density fields near the leading edge of the blade. Due to the curvature of the streamlines, a small shadow zone is formed on the pressure surface extending from slightly aft of the leading edge to about one-third of the blade chord, where the particle flow reattaches. That this very fine feature can be captured by the Eulerian method is an indication of its accuracy and robustness. It is interesting to note that a deposition-free region in precisely this position is often found on real turbine blades after operation in dirty-gas flows.

A more quantitative comparison is shown in Fig. 18 where the surface particle density and deposition rate are plotted as functions of (dimensionless) distance from the leading edge. Apart from some scatter at the leading edge on the part of the Lagrangian calculations, the agreement between the two methods is excellent, showing that the Eulerian method is eminently suited to the solution of such inertially dominated flows.

12. Conclusions

The paper has described a robust, new Eulerian calculation method for two-dimensional, non-turbulent particle flows which can be applied even in cases where large particle-free shadow zones form as a result of high particle inertia. The method includes a number of novel numerical techniques which have not been reported previously but which are essential to

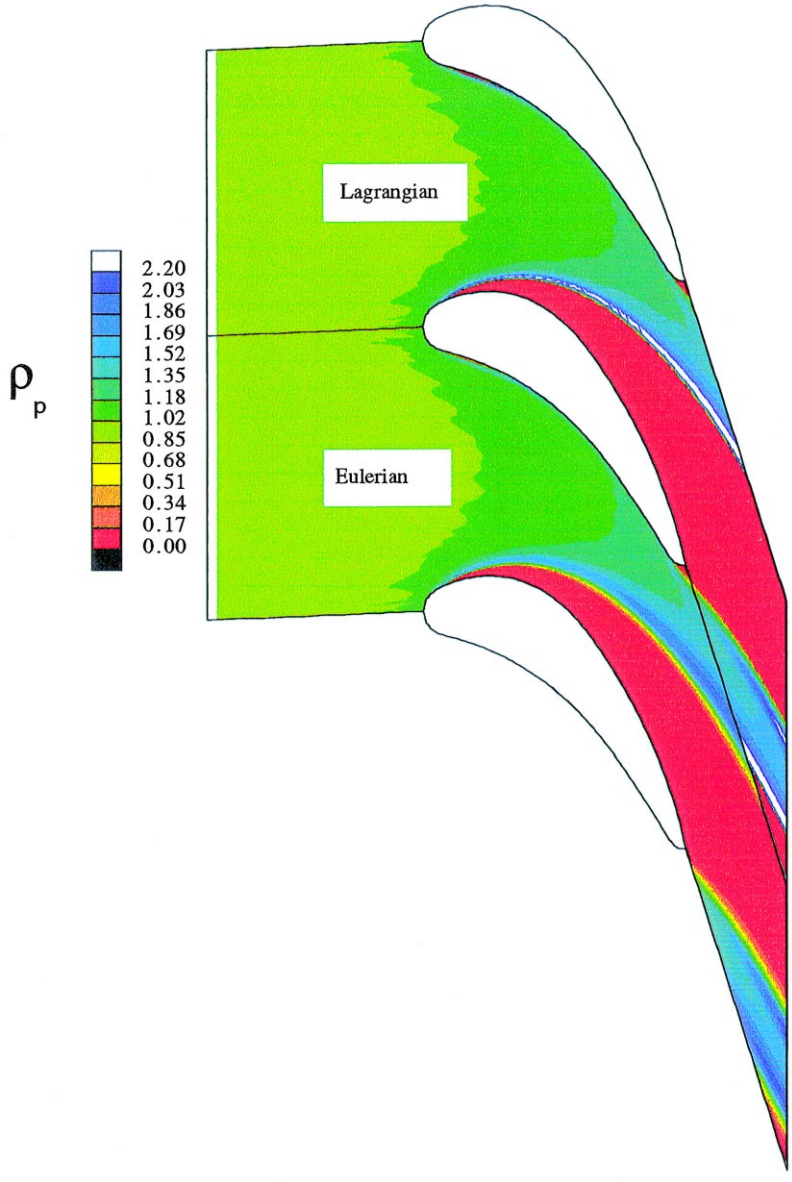

Fig. 16. Particle transport through a turbine cascade: Stokes no. = 12, Eulerian and Lagrangian calculations.

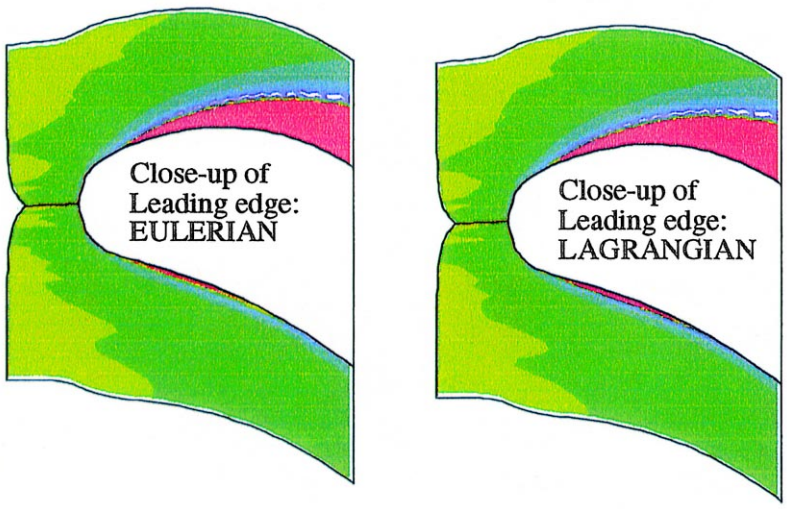

Fig. 17. Magnified view at the leading edge showing thin shadow zone on pressure surface: Stokes no. = 12, Eulerian and Lagrangian calculations.

ensure accurate representation of the physical processes, stability of the numerical method and convergence in realistic timescales (particularly for flows at very low Stokes number).

Traditionally, Lagrangian tracking methods have been recommended for many classes of dilute particle flow but this paper makes the point that they are often computationally very expensive when an accurate representation of the particle density field is required. The problem is compounded if the flowfield is three-dimensional or if a random walk element is introduced to model the response of the particles to the turbulence of the carrier fluid. The two test cases reported in this paper have shown, however, that an Eulerian method can offer a very satisfactory alternative, particularly in terms of the computational effort required for more

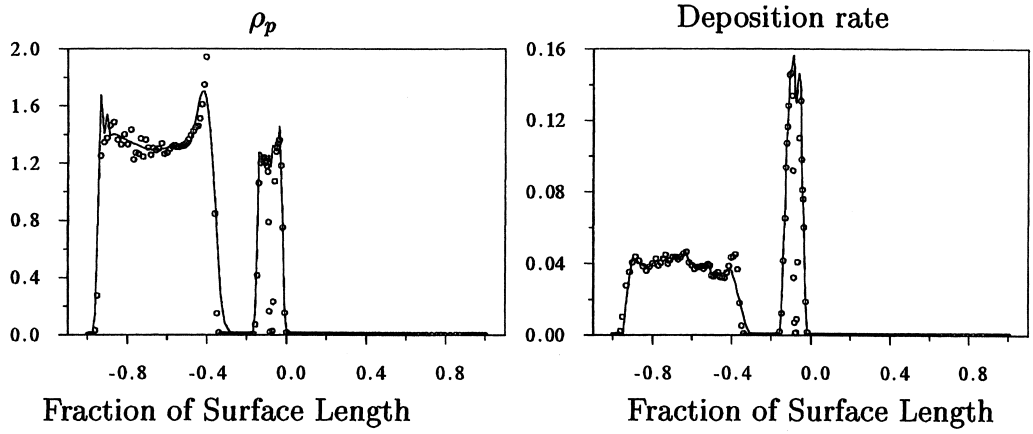

Fig. 18. Variation of particle density and deposition rate on the blade surface: Stokes no. = 12, (———) Eulerian, (●) Lagrangian. −1 to 0: pressure surface, 0 to 1: suction surface.

complex flows. Furthermore, the accuracy is excellent for many types of flow at large Stokes numbers which are normally considered to be the province of Lagrangian methods. The only major disadvantage is in handling crossing trajectories and particle reflections at solid surfaces as the Eulerian equations (couched in terms of a single-valued velocity vector) then become ill-posed. Extensions to three-dimensional and turbulent flows are possible, however, and such developments will form the basis for future work at Cambridge.

Acknowledgements

The work was carried out at the Whittle Laboratory, Cambridge University and one author (SAS) was financially supported by an EPSRC research studentship with maintenance contributions from the PowerGen Power Technology Centre, Ratcliffe-on-Soar. The authors wish to thank Dr. John Fackrell of PowerGen for his support and technical advice and Prof. Liping Xu for providing the turbine cascade gas flow predictions.

References

Crowe, C., Sommerfeld, M., Tsuji, Y., 1998. Multiphase Flows with Droplets and Particles. CRC Press, Boca Raton.

Crowe, C.T., Sharma, M.P., Stock, D.E., 1977. The particle-source-in cell (PSI-CELL) model for gas-droplet flows. Trans ASME, J. Fluids Eng 99, 325–332.

Fernandez de la Mora, J., Rosner, D., 1981. Inertial deposition of particles revisited and extended: Eulerian approach to a traditionally Lagrangian problem. Physico-Chemical Hydrodynamics 2, 1–21.

Hirsch, C., 1990. Numerical Computation of Internal and External Flows, vol. 1. Wiley-Interscience, New York, pp. 251–253.

Hoffmann, N.A., Galea, E.R., 1993. An extension of the fire-field modelling technique to include fire-sprinkler interaction. Part I: the mathematical basis. Int. J. Heat Mass Transfer 36, 1435–1444.

Hussainov, M., Kartushinsky, A., Mulgi, A., Rudi, Ü., 1996. Gas-solid flow with the slip velocity of particles in a horizontal channel. J. Aerosol Sci 27, 41–59.

Jameson, A., Schmidt, W., Turkel, E., 1981. Numerical simulation of Euler equations by finite volume methods using Runge–Kutta time stepping schemes, Fifth Computational Fluid Dynamics Conf., pp. 1–14.

Menguturk, M., Sverdrup, E.F., 1981. A theory for fine particle deposition in two-dimensional boundary layer flows and applications to gas turbines. ASME, Gas Turbine Conference and Products Show 104, 69–76.

Morsi, S.A., Alexander, A.J., 1972. An investigation of particle trajectories in two-phase flow systems. J. Fluid Mech 55, 193–208.

Ohkawa, T., Tomiyama, A., 1994. Applicability of high-order upwind difference methods to two-fluid model: examination based on a linear model equation. Numerical Methods in Multiphase Flows, ASME-FED 185, 209–215.

Osiptsov, A.N., 1984. Investigation of regions of unbounded growth of the particle concentration in disperse flows. Fluid dynamics (English translation of Izvestiya Akademii Nauk SSSR, Mechanika Zhidkosti i Gaza) 19, 378–385.

Osiptsov, A.N., 1985. Boundary layer on a blunt body in a flow of dusty gas. Fluid dynamics (English translation of Izvestiya Akademii Nauk SSSR, Mechanika Zhidkosti i Gaza) 20, 750–757.

Osiptsov, A.N., 1997. Mathematical modelling of dusty-gas boundary layers. ASME, Appl. Mech. Rev 50, 357–369.

Papervergos, P.G., Hedley, A.B., 1984. Particle deposition from turbulent flows. Chem. Engng. Res. Des 62, 275–295.

Parker, G.J., Lee, P., 1972. Studies of the deposition of sub-micron particles on turbine blades. Proc. Instn. Mech. Engrs 186, 519–526.

Saurel, R., Daniel, E., Loraud, J., 1995. Treatment of symmetry boundary conditions for two-phase dilute flows. In: Celata, G.P., Shah, R.K. (Eds.), Proc. 1st Int. Symp. on Two-Phase Flow Modelling and Experimentation, vol. 1, pp. 125–132.

Taylor, G.I., 1940. Notes on possible equipment and technique for experiments on icing on aircraft. Collected Works of G.I.Taylor 3, 236–243.

Thai-Van, D., Minier, J.P., Simonin, O., 1994. Multidimensional two-fluid model computation of turbulent dispersed two-phase flows. Numerical Methods in Multiphase Flows, ASME-FED 185, 277–291.

Valentine, J.R., Decker, R.A., 1994. Application of a Lagrangian particle tracking scheme in a body-fitted coordinate system. Numerical Methods in Multiphase Flows, ASME-FED 185, 39–46.

Wenglarz, R.A., 1981. An assessment of deposition in PBFC power plant turbines. Trans. ASME, J. Eng. Power 103, 552–559.

Yang, X., Eidelman, S., Lottati, I., 1993. Shock-wave reflection over a semi-circular cylinder in a dusty gas. AIAA Journal 31, 1737–1743.

Young, J.B., Leeming, A.D., 1997. A theory of particle deposition in turbulent pipe flow. J.Fluid Mech 340, 129–159.